

Topology of two-dimensional turbulent flows of dust and gas

Dhrubaditya Mitra^{1,*} and Prasad Perlekar^{2,†}

¹*Nordita, KTH Royal Institute of Technology and Stockholm University, Roslagstullsbacken 23, 10691 Stockholm, Sweden*

²*Tata Institute of Fundamental Research, Centre for Interdisciplinary Sciences, Hyderabad-500107, India.*

We perform direct numerical simulations (DNS) of passive heavy inertial particles (dust) in homogeneous and isotropic two-dimensional turbulent flows (gas) for a range of Stokes number, $St < 1$. We solve for the particles using both a Lagrangian and an Eulerian approach (with a shock-capturing scheme). In the latter the particles are described by a dust-density field and a dust-velocity field. We find that: The dust-density field in our Eulerian simulations have the same correlation dimension d_2 as obtained from the clustering of particles in the Lagrangian simulations for $St < 1$; the cumulative probability distribution function (CDF) of the dust-density coarse-grained over a scale r in the inertial range has a left-tail with a power-law fall-off indicating presence of voids; The energy spectrum of the dust-velocity has a power-law range with an exponent that is same as the gas-velocity spectrum except at very high Fourier modes; The compressibility of the dust-velocity field is proportional to St^2 . We quantify the topological properties of the dust-velocity and the gas-velocity through their gradient matrices, called \mathcal{A} and \mathcal{B} , respectively. Our DNS confirms that the statistics of topological properties of \mathcal{B} are the same in Eulerian and Lagrangian frames only if the Eulerian data are weighed by the dust-density. We use this correspondence to study the statistics of topological properties of \mathcal{A} in the Lagrangian frame from our Eulerian simulations by calculating density-weighed probability density functions. We further find that in the Lagrangian frame the mean value of the trace of \mathcal{A} , $\langle \text{Tr } \mathcal{A} \rangle^\rho$ is negative and its magnitude increases with St approximately as $\exp(-C/St)$ with a constant $C \approx 0.1$. The statistical distribution of different topological structures that appear in the dust flow are different in Eulerian and Lagrangian (density-weighed Eulerian) cases particularly for St close to unity. In both of these cases, for small St the topological structures have close to zero divergence and are either vortical (elliptic) or strain-dominated (hyperbolic, saddle). As St increases, the contribution to negative divergence comes mostly from saddles and the contribution to positive divergence comes from both vortices and saddles. Compared to the Eulerian case, the density-weighed Eulerian case has less inward spirals and more converging saddles. Outward spirals are the least probable topological structures in both cases.

INTRODUCTION

Particle laden flows appear in a variety of natural phenomena such as transport of aerosol, volcanic ash in atmosphere [1], raindrop formation [2], and formation of planetesimals in protoplanetary disks [3]. To describe such multiphase flows, in what follows, we shall call the particles “dust” phase and the carrier fluid “gas” phase. In many cases the suspension is dilute enough to ignore inter-particle interactions. The dynamics of particles in this limit is controlled by their size and density ρ_p relative to that of the carrier fluid ρ_f . For small particles – smaller than the dissipative scale of the flow – with $\rho_p \gg \rho_f$ (heavy particle limit), the equations of motion further simplify and the particle dynamics is determined by a single relaxation time τ_p , such that the equation of motion of a single particle is given by

$$\dot{\mathbf{X}} = \mathbf{V}, \quad (1a)$$

$$\dot{\mathbf{V}} = \frac{1}{\tau_p} [\mathbf{u}(\mathbf{X}) - \mathbf{V}]. \quad (1b)$$

Here the dot denotes time differentiation, \mathbf{X} and \mathbf{V} are respectively the position and velocity of a particle, and \mathbf{u} is the flow velocity at the particle position that is determined by solving the Navier–Stokes equation with appropriate boundary conditions. Such particles are called heavy inertial particles (HIPs).

A crucial quantity in this subject is the (binary) collision rate – mean number of collisions between dust particles per-unit-volume per-unit-time and also the probability density function (PDF) of their collisional velocities. In most cases of

practical interests, the effects of gravity (for example, leading to sedimentation of dust) is important because differently sized dust particles reach different terminal speeds under gravity; this can be the dominant term in the collision rate. But our primary interest is the effect of turbulence on the collision rate, hence gravity is ignored in the rest of this paper. Furthermore, we consider all the dust particles to have the same size (monodisperse suspension), hence the differential terminal speeds under gravity are not relevant. The collision rate is then proportional to the mean relative velocity of two dust particles separated by a distance of $2a_p$, multiplied by the probability of finding two dust particles with separation $2a_p$ where a_p is the radius of the particles. Let us first consider the latter, v.i.z., the probability of finding two dust particles at a separation less than R ; $P_2(R)$. If the particles are homogeneously distributed then $P_2(R) \sim R^d$ where d is the dimension of space. Direct numerical simulations (DNS) in the last two decades have conclusively shown [4] that in homogeneous and isotropic turbulence the heavy inertial particles show clustering, i.e., $P_2(R) \sim R^{d_2}$ with $d_2 \leq d$, a non-monotonic function of the Stokes number, $St \equiv \tau_p/t_\eta$, where t_η is the Kolmogorov time. Clearly this clustering increases the collision rate. Next consider the former, mean relative velocity of two dust particles separated by a distance R . On one hand, if the dust-velocity field is smooth and a_p is small enough, the mean relative velocity is determined by the mean value of the gradient of dust-velocity field [5]. On the other hand, if the dust-velocity field develops discontinuities, e.g., shocks, then the mean value of jumps across the discontinuities and the number density of

the discontinuities contribute to the collision rate. Either way, it is the gradient matrix of the dust-velocity field, \mathcal{A} , that plays a central role. It can be shown [6, 7] that \mathcal{A} obeys the equation:

$$\dot{A}_{ij} = \frac{1}{\tau_p} [B_{ij} - A_{ij}] - A_{ik}A_{kj} \quad (2)$$

in Lagrangian frame, i.e., when Eq. (2) is solved along the trajectory of a dust particle. Here we have assumed Einstein convention of summing of repeated indices. The matrix \mathcal{B} with component B_{ij} is the gradient-matrix of the gas-velocity, i.e., $B_{ij} \equiv \partial_j u_i$. It is now well-established [6–9] that under quite general conditions Eq. (2) may develop singularities in finite-time – called caustics. In turbulent flows \mathcal{B} and consequently \mathcal{A} are random matrices that are not necessarily Gaussian or white-in-time. Hence we must take a statistical approach in trying to understand them. To the best of our knowledge, except Ref. [10], there has been no attempt to calculate the statistical properties of the matrix \mathcal{A} in turbulent flows. It has been calculated analytically [8] in one dimensional models where \mathcal{A} and \mathcal{B} are reduced to real variables (instead of matrices) and \mathcal{B} is assumed to be a Gaussian, white-in-time, process. In this paper our aim is to study both \mathcal{B} and \mathcal{A} in turbulent flows in two spatial dimensions.

Here we limit ourselves to incompressible two-dimensional ($2D$) turbulent flows that are considered to be a minimalistic model for atmospheric and oceanic flows [11–15]. Two-dimensional turbulence is characterised by an inverse cascade of energy to length scales larger than the forcing scale and a forward cascade of enstrophy from forcing scale down to the small scales [16–18]. In general, local topological properties of a two-dimensional flow can be characterised by the trace, Tr , and the determinant, Det , of the velocity gradient matrix [19]. For an incompressible flow of gas, $\text{Tr} \mathcal{B} = 0$. Hence the flow consists of only elliptic (vortical) or saddle (strain dominated) points which are characterised in the terms of the sign of $\Lambda \equiv \text{Det} \mathcal{B}$ (also known as the Okubo-Weiss criterion [19, 20]). A statistical description of the topology of the flow is given by the PDF of $\text{Det} \mathcal{B}$ alone. Soap-film experiments [21] and numerical studies of Navier-Stokes equations [22, 23] have used Okubo-Weiss criterion to investigate the topological properties of incompressible two-dimensional turbulent flows. In the light of the discussion of the previous paragraph, it is clear that the dust-velocity is compressible even when the gas-velocity is incompressible. Hence a statistical description of the topological structures found in the dust-flow is given by the joint PDF of $\text{Det} \mathcal{A}$ and $\text{Tr} \mathcal{A}$. This is the principal objective of this paper.

More specifically, we investigate the topological properties of the dust-velocity field passively advected by the forward cascade of an incompressible two-dimensional turbulent flow. In principle, either Eulerian or Lagrangian framework (see Ref. [24] for an overview) can be used in direct numerical simulations (DNS) to calculate the gradient matrices \mathcal{A} and \mathcal{B} . In the Eulerian framework, mass and momentum balance equations are written for both the gas phase as well as the dust phase. It is straightforward to calculate the gradient matrices

\mathcal{A} and \mathcal{B} as both the gas-velocity and the dust-velocity field are available on a grid. But, note that Eq. (2) is formulated in the Lagrangian frame, and there is no a-priori reason to assume that statistical properties of \mathcal{B} or \mathcal{A} in the two frames are necessarily the same. In the Lagrangian framework the equations of motion for the gas phase remains the same but the individual inertial particle trajectories are evolved. It is straightforward to calculate \mathcal{B} at the instantaneous position of a dust particle by interpolation, but it is non-trivial to calculate \mathcal{A} – one must solve Eq. (2) on each dust particle [10]. In either Lagrangian or Eulerian framework the possibility of development of singularities in \mathcal{A} poses a numerical problem. In our Eulerian DNS we regularize this singularity by a shock-capturing scheme.

The rest of the paper is organized as follows. In section we describe our model including a summary of the numerical techniques we have used. In section we show that : (a) The dust-density field in our Eulerian simulations have the same correlation dimension d_2 as obtained from the clustering of particles in the Lagrangian simulations for $\text{St} < 1$. (b) The dust-density coarse grained over a scale r in the inertial range, ρ_r , calculated from our Eulerian DNS shows large fluctuations. We quantify these fluctuations by computing the cumulative probability distribution function (CDF), $P^C(\rho_r)$. This CDF has a left-tail with power-law fall-off that indicates presence of voids in the dust-density. (c) The energy spectrum of the dust-velocity has a power-law range with an exponent that is same as the gas-velocity spectrum except at very high Fourier modes. The spectrum of dust-density also shows a scaling range with an exponent of -1 . The compressibility of dust velocity field is proportional to St^2 . (d) The statistics of topological properties of \mathcal{B} are the same in Eulerian and Lagrangian frames only if the Eulerian data are weighed by the dust-density. We use this correspondence to calculate statistics of topological properties of \mathcal{A} in the Lagrangian frame from our Eulerian simulations by calculating density-weighted averages probability density functions. In particular, we find that: (e) The mean value of $\text{Tr} \mathcal{A}$ in the Lagrangian frame, $\langle \text{Tr} \mathcal{A} \rangle^\rho$, is negative and its magnitude increases with St approximately as $\exp(-C/\text{St})$ with a constant $C \approx 0.1$. (f) For small τ_p , $\text{Det} \mathcal{A} \approx \text{Det} \mathcal{B}$ and $\text{Tr} \mathcal{A} \approx 2\tau_p \text{Det} \mathcal{B}$. (g) The mean value of the PDF density-weighted $\text{Det} \mathcal{A}$, $\langle \text{Det} \mathcal{A} \rangle^\rho$ is negative and its magnitude increases with St approximately as $\exp(-C/\text{St})$ with a constant $C \approx 0.1$. (h) The statistical distribution of different topological structures that appear in the dust flow are different in Eulerian and density-weighted Eulerian cases particularly for St close to unity. In both of these cases, for small St the topological structures have close to zero divergence and are either vortical (elliptic) or strain-dominated (hyperbolic, saddle). As St increases, the contribution to negative divergence comes mostly from saddles and the contribution to positive divergence comes from vortices and saddles. Compared to the Eulerian case, the density-weighted Eulerian case has less inward spirals and more converging saddles. Outward spirals are the least probable topological structures in both cases. We conclude in section .

Before we conclude this introductory section let us note that

the field of dust-gas turbulence is vast. We have so far touched only those aspects of recent research that are closely related to our specific topic of interest. For a wider introduction to this subject we suggest several recent reviews [14, 24–27] and the references therein.

MODEL

To solve for the gas-velocity, we evolve the 2D incompressible Navier–Stokes (NS) equations in the vorticity-streamfunction formulation:

$$\partial_t \omega + \mathbf{u} \cdot \nabla \omega = \nu \nabla^2 \omega - \alpha \omega + f^\omega; \quad (3a)$$

$$\nabla^2 \psi = \omega. \quad (3b)$$

Here the vorticity $\omega \equiv \nabla \times \mathbf{u} \cdot \hat{e}_z$ and the streamfunction ψ is defined by $\mathbf{u} \equiv -\nabla \times (\psi \hat{e}_z)$ where \mathbf{u} is the gas-velocity, ν is the gas-viscosity, α is the Ekman drag coefficient, and we employ the Kolmogorov forcing $f^\omega = -f_0 k_f \cos(k_f x)$ that has been used in earlier experimental [29–31] and numerical [23, 28, 32, 33] studies to drive the flow. Here f_0 and k_f are the forcing amplitude and the wavenumber respectively. To model the dust phase in Lagrangian frame we solve Eq. (1). To model the dust phase in Eulerian frame we solve:

$$\partial_t \rho + \nabla \cdot (\rho \mathbf{v}) = 0, \quad (4a)$$

$$\partial_t (\rho \mathbf{v}) + \nabla \cdot (\rho \mathbf{v} \otimes \mathbf{v}) = \frac{\rho}{\tau_p} [\mathbf{u} - \mathbf{v}]. \quad (4b)$$

Here ρ is the dust-density field and \mathbf{v} is the dust-velocity field and the symbol \otimes denotes direct product of two vectors. We simultaneously numerically integrate Eqs. (1), (3), and (4) in a square box of length 2π with periodic boundary conditions. The Eulerian equations, Eq. (3) and Eq. (4), are solved with N^2 collocation points and the Lagrangian equations are solved for N_p particles. We solve Eq. (3) using a pseudo-spectral method [34]. To solve the Lagrangian equation, Eq. (1), we need to know the gas-velocity at off-grid points. This is achieved by a linear interpolation from neighbouring grid points. Because of the presence of sharp-gradients in the density field ρ , we employ the Kurganov-Tadmor scheme [35, 36] to discretize the flux terms in Eq. (4). For time integration we use a second-order Adams-Bashforth scheme. The same code, without the Eulerian description of dust phase, has been used in earlier publications [28, 37].

RESULTS

In Fig. (1) we plot representative snapshots of (a) the gas-vorticity field, and the dust-density field for (b) $St = 1.7 \times 10^{-2}$ and (c) $St = 8.6 \times 10^{-2}$. We also overplot the instantaneous position of the dust particles in (b) and (c) above. The compensated plot of the gas energy spectrum [inset of Fig. (1a)] shows a decade of forward cascade regime $E(k) \sim k^{4.2}$. The different parameters we have used in our simulations can be found in the caption of Fig. (1).

Density accumulation and Particle clustering

Earlier studies [38–42], which have tried to compare Lagrangian and Eulerian approaches to studying dust-gas multi-phase flows, have almost exclusively concentrated on comparing clustering of particles in the Lagrangian framework with the enhancement of dust-density in the Eulerian framework. In Fig. (1b) and Fig. (1c) we overlay the instantaneous positions of dust particles on a pseudocolor plot of a snapshot of the dust-density field ρ at the same time. In accord with earlier studies [40, 41], we also find that regions of clustering and regions of density accumulation lie on top of each other. Furthermore, as expected, we observe that clustering (density accumulation) is enhanced on increasing St . To make a quantitative comparison, we calculate the probability density function $P_2^E(r)$ of the dust-density from our Eulerian simulations,

$$P_2^E(r) = \left\langle \int_0^r \rho(0) \rho(\mathbf{r}') d\mathbf{r}' \right\rangle, \quad (5)$$

where the symbol $\langle \cdot \rangle$ denotes averaging of space and time in the statistically stationary state of turbulence, and compare it against the probability of finding two particles within a distance r , $P_2^L(r)$ obtained from our Lagrangian simulations. In Fig. (2a) we plot, in log-log scale, $P_2^E(r)$ and $P_2^L(r)$, for two representative values of St and in the inset we plot the corresponding local slopes. The Eulerian and the Lagrangian data agrees very well with each other. From the scaling behavior of $P_2^E(r) \sim r^{d_2}$ as $r \rightarrow 0$, we find that the exponent $d_2 \approx 2$ for $St = 0.034$ and $d_2 \approx 1.64$ for $St = 0.17$. Similar comparison was earlier made in Refs. [40, 41] in three-dimensions using the “equilibrium–Euler” approximation [43].

In Fig. (2b) we plot the density weighted PDF $P^\rho(\rho_r)$ of the dust density ρ coarse-grained over a scale, $r \equiv L/16$, which is inside the inertial range. Henceforth the superscript ρ would denote density-weighting. The Lagrangian analog of P^ρ is the quasi-Lagrangian particle number-density (averaged over a box of size r) which was calculated – for 3D turbulent flows – in Ref. [4]. Similar to Ref. [4] we find that $P^\rho \sim \delta(\rho_r)$ for small St whereas, for large St the PDF broadens and a power-law tail seem to appear as the left tail near $\rho_r \sim 1$. To investigate the left-tail in greater details, we plot in the inset of Fig. (2b) the cumulative probability distribution function $P^C(\rho_r)$ which should scale in the same way as the $P^\rho(\rho_r)$. We find two power-law regions: for very small $\rho_r < 10^{-1}$, $P^C(\rho_r) \sim \rho_r^{0.15}$ whereas for intermediate $10^{-1} < \rho_r < 1$, $P^C(\rho_r) \sim \rho_r^{1.6}$. The power-law behavior for intermediate ρ_r is consistent with the findings of Ref. [4]. The behavior at very small ρ_r is consistent with presence of voids (regions with low density).

Spectrum of dust-density and dust-velocity

Next, we plot the angle-averaged spectrum of dust-velocity and dust-density, $E_v(k)$ and $E_\rho(k)$ respectively, as a function

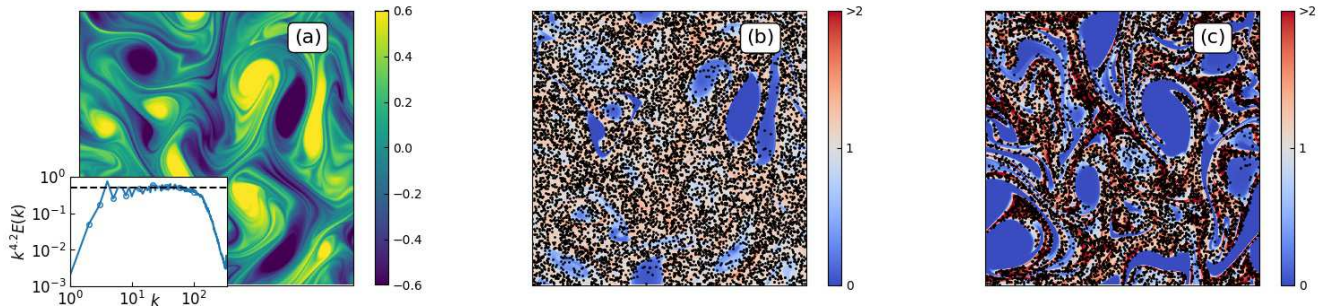


FIG. 1. Representative snapshot of the (a) gas-vorticity field and dust-density field for (b) $St = 1.7 \times 10^{-2}$ and (c) $St = 8.6 \times 10^{-2}$. In (a) we have also plotted the compensated time-averaged energy spectrum of gas-velocity. The black line indicates the $k^{-4.2}$ scaling. In (b) and (c) we have overlaid the position of dust particles from our Lagrangian simulations. We have used $N = 1024$ grid points in each direction in our Eulerian simulations, and $N_p = 10^4$ particles in Lagrangian simulations. We use $\nu = 10^{-5}$, $\alpha = 10^{-2}$, $f_0 = 5 \times 10^{-3}$ and $k_f = 4$. This generates a two-dimensional turbulent flow with a forward cascade [(a)(inset)] with $Re = 1319$ and Kolmogorov time scale $t_\eta \approx 2.9$ [28]. We choose $St = 3.4 \times 10^{-3}$, 1.7×10^{-2} , 3.4×10^{-2} , 8.6×10^{-2} , and $St = 1.7 \times 10^{-1}$.

of the Fourier mode k , in Fig. (3). The spectrum of dust-velocity follows the spectrum of gas-velocity except at very high Fourier modes. This is indeed what we expect because the dust-velocity essentially relaxes to the local gas-velocity except at high Fourier modes (small scales) where large gradients appear. The spectrum of dust-density shows a power-law with an exponent of -1 , i.e., $E_\rho(k) \sim 1/k$. This is similar to the Batchelor scaling observed for the case of passive-scalar advected by a chaotic flow. To the best of our knowledge the dust-density spectrum has not been calculated in 2D turbulence before. The compressibility of the dust flow can be quantified by calculating,

$$\kappa \equiv \frac{|\nabla \cdot \mathbf{v}|^2}{|\nabla \mathbf{v}|^2}, \quad (6)$$

which we find, consistent with [42], to be proportional to St^2 , as shown in the inset of Fig. (3).

Topological properties

The topological properties of any two-dimensional flow at a point is characterised by the two invariants of the 2×2 gradient-matrix, the trace (Tr) and the determinant (Det). Four different types of topological structures are possible. Following Ref. [44] we sketch them in Fig. (4). Along the vertical axis the trace is zero, hence two possible structures are either elliptic (center, $\text{Det} > 0$) or hyperbolic (saddle, $\text{Det} < 0$). The topological structures of \mathcal{B} lies on this line as the gas flow is incompressible. In the more general case of \mathcal{A} other topological structures are possible. Above the parabola with equation, $(\text{Det})^2 = \text{Tr}/4$ lies vortical structures. They can be either inward spirals ($\text{Tr} < 0$) or outward spirals ($\text{Tr} > 0$). Below the parabola lies the strain-dominated structures, saddles. They can be either converging ($\text{Tr} < 0$) or diverging ($\text{Tr} > 0$).

In our case the gradient matrices are \mathcal{A} , and \mathcal{B} , whose com-

ponents are defined by

$$A_{ij} \equiv \partial_j v_j, \text{ and } B_{ij} \equiv \partial_j u_i. \quad (7)$$

They are random matrices which are not necessarily Gaussian or white-in-time. Clearly, their topological properties are necessarily statistical in nature. For \mathcal{B} , the trace is zero due to incompressibility hence its statistical properties are completely described by $\Lambda \equiv \text{Det}(\mathcal{B})$. The statistical properties of \mathcal{B} as seen by the dust particles determines statistical properties of \mathcal{A} through Eq. (2). Let us first calculate the statistical properties of Λ as seen by dust particles.

Topology of the gas velocity field

In Lagrangian simulations the PDF of Λ as seen by the dust, $P^L(\Lambda)$, can be directly calculated at the off-grid location of the Lagrangian dust particles using interpolation. This PDF is plotted in Fig. (5a) for a representative value of $St = 8.6 \times 10^{-2}$. To calculate the same quantity in the Eulerian case it is not sufficient to calculate Λ at Eulerian grid points but additionally, to account for the inhomogeneities in the dust-density, we must use a density-weighted PDF $P^\rho(\Lambda)$, which is also plotted in Fig. (5a). We conclude from Fig. (5a) that these two PDFs agree well with each other. This establishes the correspondence between Eulerian and Lagrangian statistics that we shall use throughout this paper: the Lagrangian statistics of any quantity is obtained by calculating the Eulerian statistics of the same quantity weighed by the dust-density. Note that this equivalence – in whose support we shall present more results below – is established for time independent quantities only, it does not imply that a similar correspondence can be made between the correlation time of a certain quantity in Eulerian and Lagrangian frame. Earlier experiments and numerical simulations [21, 23, 28] have investigated the distribution of vortical and strain dominated regions for the case of tracers ($St = 0$). These studies show that the distribution is positively skewed indicating the prominence of vortical regions in the gas flow.

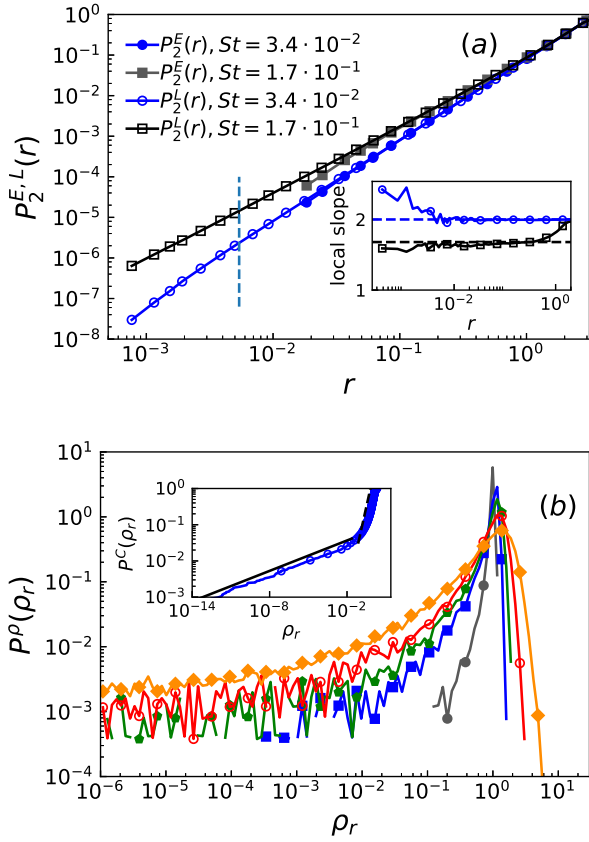


FIG. 2. (a) Log-log plot of the dust probability density function (PDF) in Eulerian $P_2^{E,L}(r)$ for $St = 3.4 \times 10^{-2}$ and $St = 0.017$. (Inset) Local slope $d_2 = d \log P_2^L(r) / d \log(r)$ analysis gives $d_2 = 2$ for $St = 3.4 \times 10^{-2}$ (blue circle) and $d_2 = 1.64$ for $St = 0.16$ (black square). (b) Log-log density-weighted PDF of the coarse grained dust-density ρ_r for different values of the Stokes number, $St = 3.4 \times 10^{-3}$ (black circle), $St = 0.017$ (blue square), $St = 0.034$ (green pentagon), $St = 0.086$ (red empty circle), and $St = 0.17$ (orange diamond). (Inset) Cumulative PDF of ρ_r for $St = 0.086$ shows that $P^C(\rho_r) \sim \rho_r^{1.6}$ for $0.1 < \rho_r < 1$ (black dashed line) and $P^C(\rho_r) \sim \rho_r^{0.15}$ for $\rho_r < 0.1$ (black line).

Since dust particles expelled out of vortical regions we expect the right tail of the PDF to decrease faster as St increases. This is indeed confirmed in Fig. (5b).

Topology of the dust velocity field

To characterise the topological properties of the dust velocity field we must use both the determinant and trace of the gradient-matrix \mathcal{A} . This can be done in a Lagrangian simulation only if for each individual Lagrangian dust particle we solve for not only its position and momentum but also for the nine independent components, A_{ij} by solving Eq. (2). So far, such a calculation has been done only in Ref [10] in three-dimensional turbulent flows. Let us start by calculating the

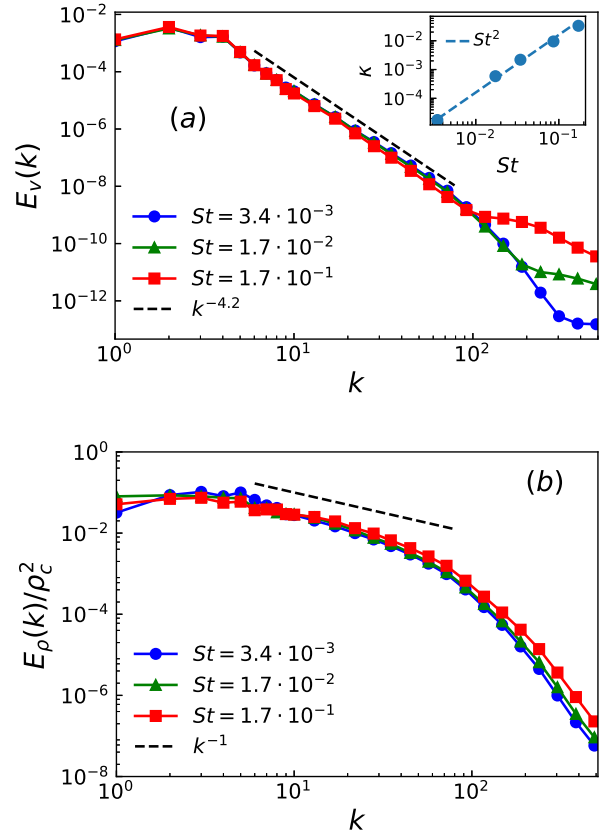


FIG. 3. Log-log plot of the spectrum of (a) dust-velocity and (b) dust-velocity for three values of St . In (a) the black line show a slope of -4.2 which is also the slope of the spectrum of gas-velocity. In (b) the black line shows a slope of -1 .

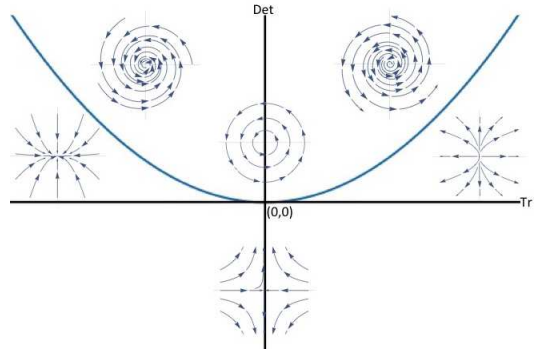


FIG. 4. A sketch of possible topological structures in the two-dimensional in the Det - Tr plane of the gradient-matrix of the flow. Above the horizontal axis ($Det > 0$), the structures are classified into: (Left-Right) Sink, Inward spiral, Center, Outward spiral, and Source. Below the horizontal axis ($Det < 0$) only saddles are possible. The parabola $(Det)^2 = Tr/4$ (blue line) marks the boundary between the vortical and non-vortical regions.

topological properties of \mathcal{A} first in the Eulerian framework.

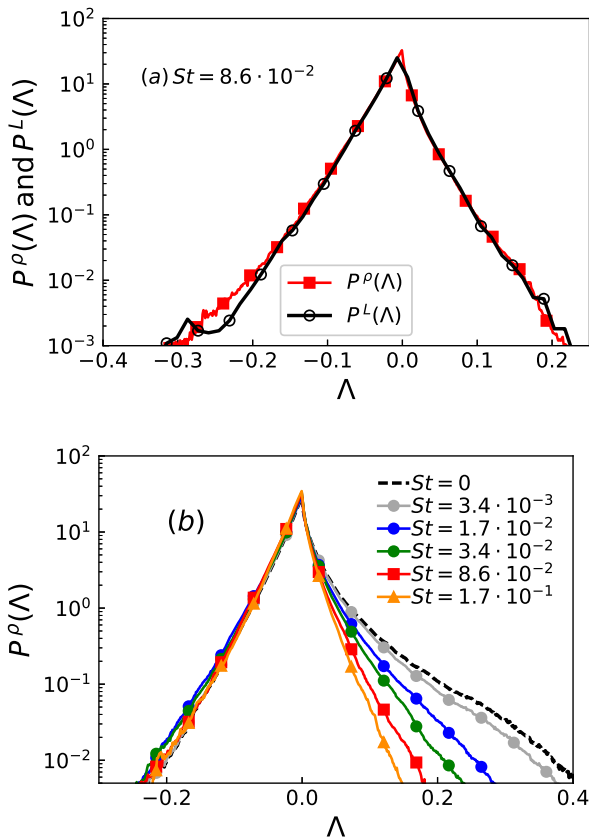


FIG. 5. (a) The dust-density weighed PDF of Λ calculated from Eulerian simulations, $P^\rho(\Lambda)$, and the Lagrangian PDF of Λ , $P^L(\Lambda)$; $\Lambda \equiv \text{Det } \mathcal{B}$. (b) The dust-density weighed PDF of Λ , $P^\rho(\Lambda)$ calculated from Eulerian simulations for several different values of St .

Topology of dust velocity in Eulerian simulations

In Fig. (6a) and Fig. (6b) we plot respectively the PDF of $\text{Det } \mathcal{A}$ and $\text{Tr } \mathcal{A}$ for several different values of St . We find that $P[\text{Det } \mathcal{A}]$ depends very weakly on St ; whereas $P[\text{Tr } \mathcal{A}]$ is negatively skewed and the distribution broadens as St increases. Both these results can be understood by noting that for small τ_p , the dust velocity \mathbf{v} can be expanded in powers of τ_p as $\mathbf{v} = \mathbf{u} - \tau_p D\mathbf{u}/Dt + O(\tau_p^2)$. It is then easy to show that to the leading order $\text{Det } \mathcal{A} \approx \text{Det } \mathcal{B}$ [note that $\text{Det } \mathcal{A} = \text{Det } \mathcal{B}$ for $\tau_p = 0$] and $\text{Tr } \mathcal{A} = 2\tau_p \text{Det } \mathcal{B}$. Thus, we expect that $P[\text{Det } \mathcal{A}] = P(\Lambda)$ for small St , which is indeed confirmed in Fig. (6a). On rescaling $\text{Tr } \mathcal{A}$ by $2\tau_p$ we find a reasonable collapse for small St in Fig. (6c). The distributions calculated above are projections of the joint probability distribution $Q[\text{Tr } \mathcal{A}, \text{Det } \mathcal{A}]$ on either $\text{Det } \mathcal{A} = 0$ or $\text{Tr } \mathcal{A} = 0$ axis and cannot distinguish between different types of topological structures in the flow (see Fig. (4)). To investigate the detailed flow topology, we now plot $Q[\text{Tr } \mathcal{A}, \text{Det } \mathcal{A}]$ for three different values of St in Fig. (7). For small values of $St = 3.4 \times 10^{-3}$, $\text{Tr } \mathcal{A} \approx 0$ and the Q is concentrated along the vertical axis.

On increasing the St , the joint pdf becomes broader and tilts clockwise; this is indeed what we expect because for small St ; $\text{Det } \mathcal{A} \approx \text{Tr } \mathcal{A}/(2\tau_p)$. In terms of topological structures, this implies that we get more diverging spirals and converging saddles in the flow and less of converging spirals and diverging saddles. It is the converging part that contributes to the increase in dust-density and this comes from the saddles, which are the strain-dominated points. As the St is increases further the joint PDF, Q gets wider and it does not any longer satisfy the simple relation: $\text{Det } \mathcal{A} \approx \text{Tr } \mathcal{A}/(2\tau_p)$, but the general trend among the different topological structures remain the same.

Topology of density-weighted dust velocity

We have shown before that the Lagrangian statistical properties of Λ can be calculated from the Eulerian simulations by calculating the density-weighted statistical properties. Motivated by this agreement, we now calculate the density-weighted statistical properties of $\text{Det } \mathcal{A}$ and $\text{Tr } \mathcal{A}$ from our Eulerian simulations and claim that these are the same result as would have been obtained by a Lagrangian simulation. In Fig. (8a) and Fig. (8b) we plot respectively the density-weighted PDF of the determinant of \mathcal{A} , $P^\rho[\text{Det } \mathcal{A}]$ and the trace of \mathcal{A} , $P^\rho[\text{Tr } \mathcal{A}]$ for several values of St . We find that on increasing St the right tail of $P^\rho[\text{Det } \mathcal{A}]$ systematically decreases. This can be understood by first remembering that we have already argued in the earlier section, $P[\text{Det } \mathcal{A}] \approx P[\text{Det } \mathcal{B}]$ in the Eulerian framework. This argument works equally well in the Lagrangian framework too, hence we expect that, $P^\rho[\text{Det } \mathcal{A}] \approx P^\rho[\Lambda]$. It has been argued and confirmed from simulations [45] that heavy inertial particles are ejected from vortices, hence as St increases the dust particles sample less and less the strain-dominated regions ($\Lambda > 0$), hence the right tail of $P^\rho[\text{Det } \mathcal{A}]$ decreases.

Next we plot the PDF of $\text{Tr } \mathcal{A}$ in Fig. (8b) for several different values of St . This PDF is of particular interest. The presence of singularities (caustics) would imply that the trace of \mathcal{A} would blow-up. In our simulations we have used a shock-capturing scheme to regularize these singularities, hence we are not going to find any blow-up in our simulations. Although, we may find signature of the singularities in large negative values of $\text{Tr } \mathcal{A}$. We see in Fig. (8b) that the PDF of $\text{Tr } \mathcal{A}$ has a shallower tail on the negative side than on the positive side. We quantify this by calculating the mean value of this PDF, $\langle \text{Tr } \mathcal{A} \rangle^\rho$, as a function of St [see Fig. (8c)]. Analytical calculations in a simple model [8] has shown that the frequency of caustics increases with St as $\exp(-C/St)$ with a constant C . We find that this expression is provides reasonable fit to our data on $\langle \text{Tr } \mathcal{A} \rangle^\rho$ versus St with $C \approx 0.1$.

Finally, we plot the density-weighted joint probability distribution $Q^\rho[\text{Tr } \mathcal{A}, \text{Det } \mathcal{A}]$, for three different values of St , in Fig. (9). By comparing these figures against Eulerian joint PDF, $Q[\text{Tr } \mathcal{A}, \text{Det } \mathcal{A}]$ plotted in Fig. (7) we find how the topological structures change between the Eulerian and the Lagrangian frames. Compared to the Eulerian case, in the La-

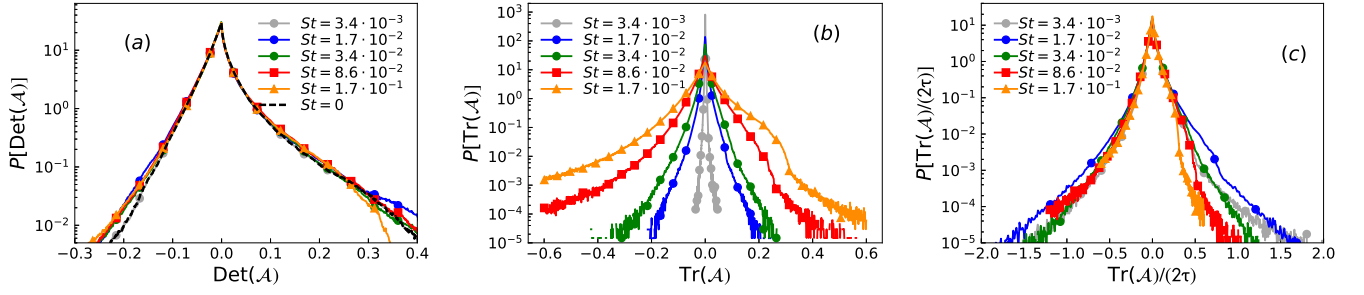


FIG. 6. (a) Probability distribution $P[\text{Det } \mathcal{A}]$ versus \mathcal{A} for different Stokes numbers. Note that $P[\text{Det } \mathcal{A}]$ does not change appreciably on changing St ; (b) $P[\text{Tr } \mathcal{A}]$ versus $\text{Tr } \mathcal{A}$ for different values of St . (c) $P[\text{Tr } \mathcal{A}/2\tau_p]$ versus $\text{Tr } \mathcal{A}/2\tau_p$ overlap for different values of Stokes number, St .

grangian (i.e., the density-weighted) case we find a qualitative change: there are less spiral structure and more saddles, and it is more probable to have converging saddles.

CONCLUSION

We characterised the topological structures that appear in homogeneous and isotropic turbulent flows of dust and gas. The gas flow is assumed to be incompressible but the flow of the dust is compressible, hence is more rich in topological structures. The topological properties of any two-dimensional flow can be characterised by the trace and the determinant of its gradient matrix. As we are dealing with a turbulent flow the matrices we deal with are random matrices, their topological properties are necessarily statistical. Earlier analytical studies [6, 8] have suggested that the flow of dust develops singularities – one or more element of the gradient-matrix, \mathcal{A} can blow-up – but the nature of such singularities in either two or three dimensions has not been elucidated. Direct numerical simulations necessarily introduces regularisation of such blow-ups – our shock-capturing scheme – hence cannot probe the blow-up directly. Within this limitation, we, for the first time, have characterised the statistics of the topological structures found in the dust velocity. We have done this in Eulerian framework, and used dust-density-weighted quantities to translate our Eulerian results to Lagrangian ones. The singularities of \mathcal{A} should disappear as $St \rightarrow 0$. Analytical results in one-dimensional models suggest that the number of blow-ups should increase as $\exp(-C/St)$, with a positive constant C . To the best of our knowledge, Ref. [10], is the only work that tried to check this result against Lagrangian DNS in three dimensions. The nature of our simulations do not allow us to directly calculate this quantity, however we have used the $\langle \text{Tr } \mathcal{A} \rangle_\rho$ as a proxy of this quantity – and have found reasonable agreement.

A summary of the other results follows: (a) The dust-density field in our Eulerian simulations have the same correlation dimension d_2 as obtained from the clustering of particles in the Lagrangian simulations for $St < 1$. (b) The dust-density

coarse grained over a scale r in the inertial range, ρ_r , calculated from our Eulerian DNS shows large fluctuations. We quantify these fluctuations by computing the cumulative probability distribution function (CDF), $P^C(\rho_r)$. This CDF has a left-tail with power-law fall-off that indicates presence of voids in dust-density. (c) The energy spectrum of the dust-velocity has a power-law range with an exponent that is same as the gas-velocity spectrum except at very high Fourier modes. The spectrum of dust-density also shows a scaling range with an exponent of -1 . (d) The compressibility of dust velocity field is proportional to St^2 . (e) The statistics of topological properties of \mathcal{B} are the same in Eulerian and Lagrangian frames only if the Eulerian data are weighed by the dust-density. We use this correspondence to calculate statistics of topological properties of \mathcal{A} in the Lagrangian frame from our Eulerian simulations by calculating density-weighted averages probability density functions. In particular, we find that: (e) The mean value of $\text{Tr } \mathcal{A}$ in the Lagrangian frame, $\langle \text{Tr } \mathcal{A} \rangle_\rho$, is negative and its magnitude increases with St approximately as $\exp(-C/St)$ with a constant $C \approx 0.1$. (b) For small τ_p , $\text{Det } \mathcal{A} \approx \text{Det } \mathcal{B}$ and $\text{Tr } \mathcal{A} \approx 2\tau_p \text{Det } \mathcal{B}$. (f) The mean value of the PDF density-weighted $\text{Det } \mathcal{A}$, $\langle \text{Det } \mathcal{A} \rangle_\rho$ is negative and its magnitude increases with St approximately as $\exp(-C/St)$ with a constant $C \approx 0.1$. (g) The statistical distribution of different topological structures that appear in the dust flow are different in Eulerian and density-weighted Eulerian cases particularly for St close to unity. In both of these cases, for small St the topological structures have close to zero divergence and are either vortical (elliptic) or strain-dominated (hyperbolic, saddle). As St increases, the contribution to negative divergence comes mostly from saddles and the contribution to positive divergence comes from vortices and saddles. Compared to the Eulerian case, the density-weighted Eulerian case has less inward spirals and more converging saddles. Outgoing spirals are the least probable topological structures in both cases.

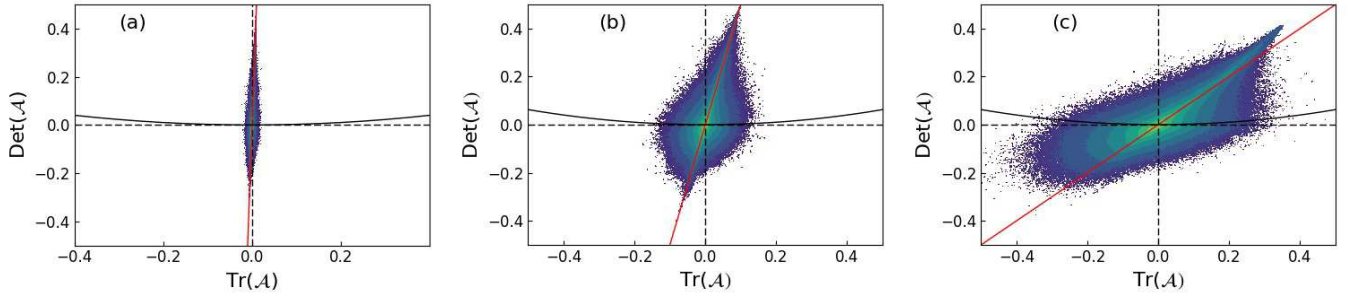


FIG. 7. Joint PDF $Q[\text{Tr } \mathcal{A}, \text{Det } \mathcal{A}]$ for $St = 3.4 \times 10^{-3}$ (a), $St = 0.017$ (b), and $St = 0.17$ (c). The red line is the equation $\text{Det } \mathcal{A} = \text{Tr } \mathcal{A}/2\tau_p$.

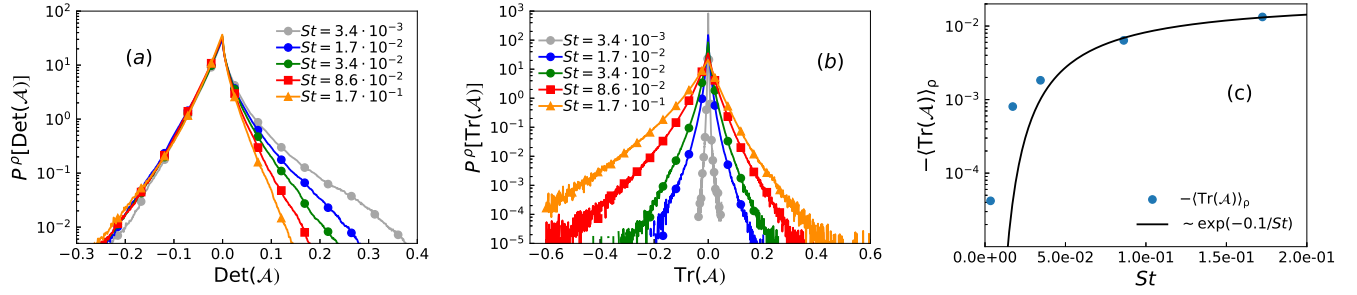


FIG. 8. Density-weighted PDFs, $P^\rho[\text{Det } \mathcal{A}]$ (a), and $P^\rho[\text{Tr } \mathcal{A}]$ (b) for different values of St . (c) The negative of the density-weighted mean of the trace of \mathcal{A} , $-\langle \text{Tr } \mathcal{A} \rangle^\rho$ as a function of St . The continuous line in the figure is the expression $\exp(-0.1/St)$

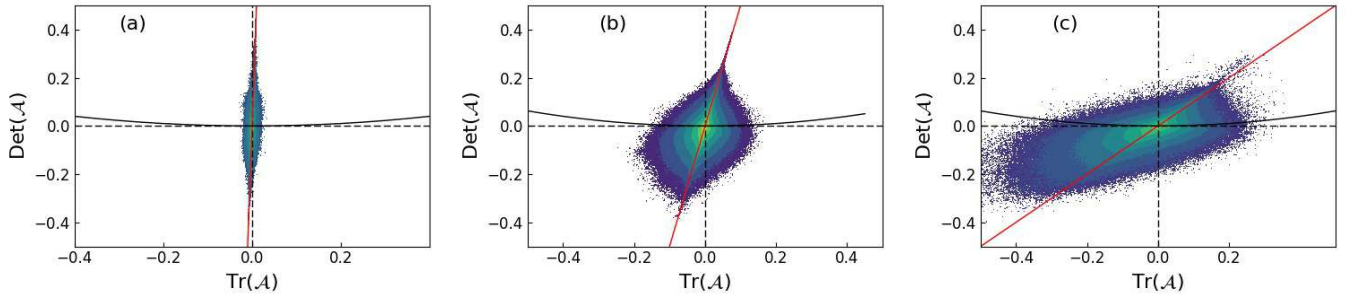


FIG. 9. Density-weighted joint PDFs $Q^\rho[\text{Tr } \mathcal{A}, \text{Det } \mathcal{A}]$ for $St = 3.4 \times 10^{-3}$ (a), $St = 0.017$ (b), and $St = 0.17$ (c). The red line is the function $\text{Det } \mathcal{A} = \text{Tr } \mathcal{A}/2\tau_p$. The wide parabola is the line $(\text{Det } \mathcal{A})^2 = \text{Tr } \mathcal{A}/4$.

ACKNOWLEDGEMENT

DM is supported by the grant Bottlenecks for particle growth in turbulent aerosols from the Knut and Alice Wallenberg Foundation (Dnr. KAW 2014.0048). DM thanks Akshay Bhatnagar for useful discussions.

* dhruba.mitra@gmail.com

† perlekar@tifrh.res.in

- [1] J.F. Kok, E.J.R. Parteli, T.I. Michaels, and D.B. Karam, “The physics of wind-blown sand and dust,” *Rep. on Prog. in Phys.* **75**, 106901 (2012).
- [2] H.R. Pruppacher and J.D. Klett, *Microphysics of Clouds and Precipitation*, Vol. 18 (Springer Science & Business Media, 2010).
- [3] P. J. Armitage, *Astrophysics of Planet Formation* (Cambridge University Press, Cambridge, UK, 2010).
- [4] J. Bec, L. Biferale, M. Cencini, A. Lanotte, S. Musacchio, and F. Toschi, “Heavy particle concentration in turbulence at dissipative and inertial scales,” *Phys. Rev. Lett.* **98**, 084502 (2007).
- [5] P. G. Saffman and J. S. Turner, “On the collision of drops in turbulent clouds,” *J. Fluid Mech.* **1**, 16–30 (1956).
- [6] G. Falkovich, A. Fouxon, and M. Stepanov, “Acceleration of rain initiation by cloud turbulence,” *Nature, London* **419**, 151–154 (2002).
- [7] M. Wilkinson and B. Mehlig, “Caustics in turbulent aerosols,” *Europhys. Lett.* **71**, 186 (2005).
- [8] M. Wilkinson, B. Mehlig, and V. Bezuglyy, “Caustic activation of rain showers,” *Physical review letters* **97**, 048501 (2006).
- [9] K Gustavsson and B Mehlig, “Relative velocities of inertial particles in turbulent aerosols,” *Journal of Turbulence* **15**, 34–69 (2014).
- [10] G. Falkovich and A. Pumir, “Sling effect in collisions of water droplets in turbulent clouds,” *J. Atmos. Sci.* **64**, 4497–4505 (2007).
- [11] G. Boffetta and R. E. Ecke, “Two-dimensional turbulence,” *J. Fluid Mech.* **44**, 427 (2012).
- [12] S.D. Danilov and D. Gurarie, “Quasi-two-dimensional turbulence,” *Physics-Usppekhi* **43**, 863–900 (2000).
- [13] N. Schorghofer and S.T. Gille, “Statistics of velocity gradients in two-dimensional navier-stokes and ocean turbulence,” *Phys. Rev. E* **65**, 026307 (2002).
- [14] R. Pandit, P. Perlekar, and S. S. Ray, “Statistical properties of turbulence: An overview,” *Pramana* **73**, 179 (2009).
- [15] R. Pandit, D. Banerjee, A. Bhatnagar, M. Brachet, A. Gupta, D. Mitra, N. Pal, P. Perlekar, S.S. Ray, V. Shukla, and D. Vincenzi, “An overview of the statistical properties of two-dimensional turbulence in fluids with particles, conducting fluids, fluids with polymer additives, binary-fluid mixtures, and superfluids,” *Phys. Fluids* **29**, 111112 (2017).
- [16] R.H. Kraichnan, “Inertial ranges in two-dimensional turbulence,” *Phys. Fluids* **10**, 1417–1423 (1967).
- [17] C.E. Leith, “Diffusion approximation for two-dimensional turbulence,” *Phys. Fluids* **11**, 671 (1968).
- [18] G. K. Batchelor, “Computation of the energy spectrum in homogeneous two-dimensional turbulence,” *Phys. Fluids Suppl. II* **12**, 233 (1969).
- [19] A.B. Okubo, “Horizontal dispersion of floatable particles in the vicinity of velocity singularities such as convergences,” *Deep-Sea Res.* **17**, 445 (1970).
- [20] J. Weiss, “The dynamics of enstrophy transfer in two-dimensional turbulence,” *Physica D* **48**, 273 (1992).
- [21] M. Rivera, X.L. Wu, and C. Yeung, “Universal distribution of centers and saddles in two-dimensional turbulence,” *Phys. Rev. Lett.* **87**, 044501 (2001).
- [22] C. Basdevant and T. Philipovitch, “On the validity of “weiss criterion” in two-dimensional turbulence,” *Physica D* **73**, 17 (1994).
- [23] P. Perlekar and R. Pandit, “Statistically steady turbulence in soap films: Direct numerical simulations with ekman friction,” *New J. Phys.* **11**, 073003 (2009).
- [24] S. Balachandar and J.K. Eaton, “Turbulent dispersed multiphase flow,” *Ann. Rev. Fluid Mech.* **42**, 111 (2010).
- [25] F. Toschi and E. Bodenschatz, “Lagrangian properties of particles in turbulence,” *Annu. Rev. Fluid Mech.* **41**, 375 (2009).
- [26] A. Pumir and M. Wilkinson, “Collisional aggregation due to turbulence,” *Annu. Rev. Condens. Matter Phys.* **7**, 141–170 (2016).
- [27] K Gustavsson and B Mehlig, “Statistical models for spatial patterns of heavy particles in turbulence,” *Adv. Phys.* **65**, 1–57 (2016).
- [28] P. Perlekar, S.S. Ray, D. Mitra, and R. Pandit, “Persistence problem in two-dimensional fluid turbulence,” *Phys. Rev. Lett.* **106**, 054501 (2011).
- [29] J.M. Burgess, C. Bizon, W.D. McCormick, J.B. Swift, and H.L. Swinney, “Instability of the kolmogorov flow in a soap film,” *Phys. Rev. E* **60**, 715 (1999).
- [30] M.K. Rivera, Ph.D. thesis (2001).
- [31] J. Tithof, B. Suri, R.V. Pallantla, R.O. Girgoriev, and M.F. Schatz, “Bifurcations in a quasi-two-dimensional kolmogorov-like flow,” *J. Fluid Mech.* **828**, 837 (2017).
- [32] N. Platt, L. Sirovich, and N. Fitzmaurice, “An investigation of chaotic kolmogorov flows,” *Phys. Fluids A* **3**, 681–696 (1991).
- [33] Y-K. Tsang, E. Ott, T.M. Antonsen, and P.N. Guzdar, “Intermittency in two-dimensional turbulence with drag,” *Physical Review E* **71**, 066313 (2005).
- [34] C. Canuto, M. Y. Hussaini, A. Quarteroni, and T. A. Zang, *Spectral methods in Fluid Dynamics* (Springer-Verlag, Berlin, 1988).
- [35] J. Balbás and E. Tadmor, “CENTPACK,” online at <http://www.cscamm.umd.edu/centpack/software> (2006), available at: <http://www.cscamm.umd.edu/centpack/software>.
- [36] A. Kurganov and E. Tadmor, “New high-resolution central schemes for nonlinear conservation laws and convection-diffusion equations,” *J. Comp. Phys.* **160**, 241–282 (2000).
- [37] S.S. Ray, D. Mitra, P. Perlekar, and R. Pandit, “Dynamic multiscaling in two-dimensional fluid turbulence,” *Phys. Rev. Lett.* **107**, 184503 (2011).
- [38] O.A. Druzhinin and S. Elghobashi, “Direct numerical simulations of bubble-laden turbulent flows using the two-fluid formulation,” *Phys. Fluids* **10**, 685 (1998).
- [39] P. Février, O. Simonin, and K.D. Squires, “Partitioning of particle velocities in gas-solid turbulent flows into a spatially uncorrelated random distribution: theoretical formalism and numerical study,” *J. Fluid Mech.* **533**, 1 (2005).
- [40] S.L. Rani and S. Balachandar, “Evaluation of the equilibrium eulerian approach for the evolution of particle concentration in isotropic turbulence,” *Int. J. Multiph. Flow* **29**, 1793 (2003).
- [41] S.L. Rani and S. Balachandar, “Preferential concentration of particles in isotropic turbulence: a comparison of the lagrangian and the equilibrium eulerian approaches,” *Powder Technology* **141**, 109 (2004).
- [42] G. Boffetta, A. Celani, F. De Lillo, and S. Musacchio, “The eulerian description of dilute collisionless suspension,” *Europhys. Lett.* **78**, 14001 (2007).

- [43] Within the equilibrium–Euler approximation one assumes that τ_p is small hence the dust velocity is approximated to be $\mathbf{v} \equiv \mathbf{u} - \tau D\mathbf{u}/Dt$.
- [44] M.W. Hirsch, S. Smale, and R.L. Devaney, *Differential equations, dynamical systems, and an introduction to chaos* (Elsevier Academic Press, California, USA, 2004).
- [45] J. Bec, “Multifractal concentrations of inertial particles in smooth random flows,” *J. Fluid Mech.* **528**, 255 (2005).